Acta Crystallographica Section A
Foundations of Crystallography
ISSN 0108-7673

Received 24 November 2006
Accepted 17 January 2007

Characterization of pyramidal inversion boundaries in Sb_2O_3-doped ZnO by using electron back-scattered diffraction (EBSD)

Wook Jo,* Chan Park and Doh-Yeon Kim

Department of Materials Science and Engineering, Seoul National University, Seoul 151-744, Korea. Correspondence e-mail: whdnr01@snu.ac.kr

The composition planes of the inversion boundary induced by the addition of Sb_2O_3 to ZnO ceramics were analyzed crystallographically by the application of electron back-scattered diffraction (EBSD) analysis and stereographic projection techniques. The inversion boundary was determined to consist of three discrete composition planes, {0001}, $\{10\bar{1}1\}$, $\{10\bar{1}0\}$.

1. Introduction

During the fabrication of Bi_2O_3-doped ZnO varistor ceramics, a careful control of grain growth during sintering is required because their breakdown voltage is critically dependent upon the average grain size. A common procedure for this purpose is to use additives such as Sb_2O_3 (Senda & Bradt, 1991; Rečnik *et al.*, 2001; Daneu *et al.*, 2003) or SnO_2 (Daneu *et al.*, 2000; Daneu & Bernik, 2001), which are known to influence the grain growth of ZnO grains.

The long-standing alleged mechanism for growth inhibition has been the Zener dragging effect by the spinel second phase formed at the boundary. However, Daneu *et al.* (2003) recently proposed that the growth of ZnO is not hindered but promoted by the addition of Sb_2O_3. Specifically, the final grain size is controlled by the number of rapidly growing ZnO grains due to the reduction of the energy barrier for the two-dimensional nucleation process by the presence of the inversion boundary (IB) that is induced by the addition of Sb_2O_3. Note that the grains containing such two-dimensional imperfections can have a coarsening advantage as is demonstrated in $BaTiO_3$ (Yoo *et al.*, 1997; Kang *et al.*, 2000; Kang & Kim, 2000) and PMN-PT ceramics (Chung *et al.*, 2002*a*,*b*, 2004). In short, when Sb_2O_3 is doped, many ZnO grains with IB are formed and impinge upon each other in the early stage of heat treatment so that the resultant grain size can be rather fine and uniform.

In this regard, understanding the physicochemical nature of IB is essential in controlling the grain growth of ZnO ceramics. IB, where the inversion of the symmetry of a polar crystal takes place, is a rather commonly appearing defect which has been reported in a number of materials such as compound semiconductors, crystals of the wurtzite structure and even rhombohedral crystals (Austerman, 1962; Holt, 1969; Snykers *et al.*, 1971; Morizane, 1977; Petroff, 1986; Pirouz & Powell, 1987; Romano *et al.*, 1987). Owing to its frequent occurrence, the crystallographic aspects, atomic structure and chemical features of the IB in various materials have been investigated extensively.

Recently, we have shown through the analysis of orientation-dependent etching characteristics that the IB in ZnO is a basal twin, and the twin plane that separates the crystal crystallographically corresponds to (0001). It was further demonstrated that the twin boundary has a so-called 'head-to-head ($\rightarrow|\leftarrow$)' configuration (Jo *et al.*, 2005). Here, the direction of the polar vector is defined from the O-terminating $-C$ basal plane $(000\bar{1})$ to the Zn-terminating $+C$ basal plane (0001).

However, analyses on the composition planes that actually separate the twinned ZnO are rare in the literature. Most studies have been directed toward the coherent (0001) composition plane (Kim & Goo, 1990; Rečnik *et al.*, 2001), although it has usually been observed that the composition planes consist not only of (0001) but of two additional unidentified planes (Daneu *et al.*, 2003). In that the physicochemical features due to the presence of IB are more closely related to the composition planes than to the twin plane, a complete identification of the other composition planes is warranted.

The purpose of the present study is to develop a simple method to determine the crystallographic features of the composition planes of the IB in ZnO macroscopically, and discuss the underlying principles. The current method revealed that the composition planes of IB are {0001}, $\{10\bar{1}1\}$ and $\{10\bar{1}0\}$.

2. Experimental procedure

The overall experimental procedure was identical with that described elsewhere (Jo *et al.*, 2005). ZnO and Bi_2O_3 powders (both are 99.99% pure and from Aldrich Chemical Co., Milwaukee, WI, USA) and Sb_2O_3 powders (98% pure S.P.C. GR reagent, Shinyo Pure Chemicals Co. Ltd, Osaka, Japan)

were used as starting powders. Powder mixtures of 99.7 ZnO–0.25 Bi_2O_3–0.05 Sb_2O_3 (in mol%) were prepared by ball-milling for 4 h in ethanol. After drying, the powders were hydrostatically pressed into cylindrical compacts at 200 MPa. The compacts were heated at a rate of 5 K min^{-1} and sintered at 1473 K for 3 h. For sintering, the compacts were put together with the same powder in a closed platinum crucible to minimize the evaporation of Bi_2O_3.

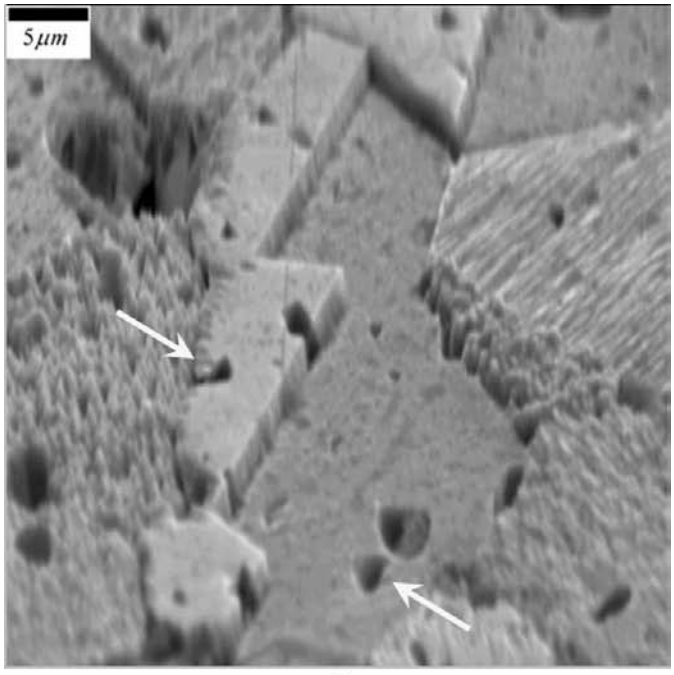

(*a*)

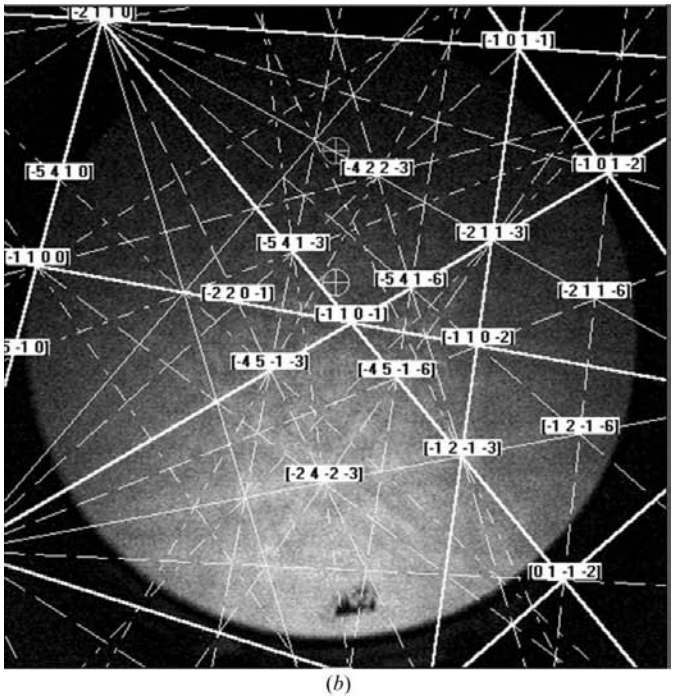

(*b*)

Figure 1
(*a*) SEM image showing a typical ZnO grain with IB. (*b*) Kikuchi pattern of the ZnO grain in (*a*).

The cross section of the sintered specimen was mirror-polished and etched chemically by dilute HCl with a small amount of HF for 20 s at room temperature. Scanning electron microscopy (SEM, JSM-6330F, JEOL, Japan) was used for the microstructure observation. The orientation for ZnO grains was determined using electron back-scattered diffraction (EBSD, Oxford/Link Opal, England). To avoid any possible build up of electron charges, amorphous carbon about 8 nm thick was sputtered onto the polished surface of each specimen. The Kikuchi patterns were obtained with the accelerating voltage and specimen tilt being 20 kV and 70°, respectively.

3. Results and discussion

Fig. 1(*a*) is a typical SEM image of a ZnO grain with IB. It can be noticed that the inversion boundary has three distinct composition planes. EBSD analysis was performed, and the obtained Kikuchi pattern is presented in Fig. 1(*b*). Note the Kikuchi pattern from both parts of the grain separated by the IB is identical. This indicates that the grain is twinned with respect to the basal plane, since the polarity cannot be differentiated by the Kikuchi pattern given by EBSD. From the Kikuchi pattern, the orientation of the sample normal was determined to be $(2\bar{1}\bar{1}2)$. Fig. 2(*a*) is a stereographic projection of the ZnO grain in Fig. 1(*a*) with the major poles of the hexagonal system, {0001}, $\{10\bar{1}0\}$ and $\{2\bar{1}\bar{1}0\}$.

The composition plane for the major portion of the IB (which will be referred to as IB-1, hereafter) can be easily determined from the etch pits indicated by the arrows in Fig. 1(*a*). As has been previously demonstrated (Jo *et al.*, 2005), the presence of triangular etch pits whose apexes point to each other across the IB indicates that the composition plane of the corresponding IB is (0001). Since the crystallography of IB-1 is quite straightforward, the focus here will be on characterizing the other two parts of the IB (IB-2 and IB-3), as is described in a schematic figure of the ZnO grain (see Fig. 2*b*).

The determination of the non-basal portions of the IB such as IB-2 and IB-3 is more or less complicated since a single

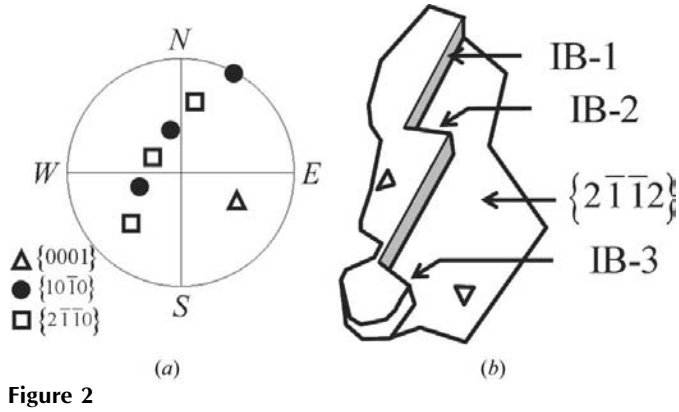

(*a*) (*b*)

Figure 2
(*a*) Stereographic projection of the ZnO grain shown in Fig. 1(*a*) with major poles of the hexagonal system. (*b*) Schematic illustration for the notation used in the current analysis.

solid/solid interface generally requires as many as five degrees of freedom (DOF) to be defined crystallographically. When we designate the normal vectors of crystallographic planes with the same Miller index chosen arbitrarily from both crystals as $\hat{n}_1$ and $\hat{n}_2$, it is possible to bring two crystals into a single coordinate system by the use of three DOFs: $\hat{n}_1$, $\hat{n}_2$ and the misorientation angle ψ that refers to the angle between $\hat{n}_1$ and $\hat{n}_2$. Then, the direction of the normal vector of the common plane, which is perpendicular both to $\hat{n}_1$ and $\hat{n}_2$, is the common axis, and the plane, which contains the common axis and is placed at the same angular distance from $\hat{n}_1$ and $\hat{n}_2$, is the symmetry dividing plane.

For this simple physical concept to be applied in practice, a certain level of mathematical exploitation is needed. One of the most common procedures is to employ Euler's rotation theorem, which states that any arbitrary rotation can be described by three angular parameters, namely $(\varphi_1, \Phi, \varphi_2)$. φ_1 denotes the rotation about the z axis, Φ the rotation about the x axis and φ_2 the rotation about the transformed z axis. What can be determined by the application of Euler's rotation theorem is the symmetry dividing plane of two misoriented crystals.

However, the actual dividing plane generally deviates from the symmetry dividing plane except for the case of the symmetrical tilt grain boundaries (STGB). As a consequence, two more DOFs, such as an appropriate amount of tiling and twisting of the symmetry dividing plane, are required to adjust the deviation. These two remaining DOFs are usually represented by two angular parameters that are needed to specify the spatial orientation of the actual dividing plane with respect to the symmetry dividing plane: θ (azimuthal angle) and ϕ (polar angle). To define IB-2 and IB-3, therefore, we should determine all those five macroscopic DOFs.

Three Euler angles can be determined from the standard stereographic diagram presented in Fig. 2(*a*) because the construction of a pole figure by EBSD analysis is based on the Euler angles. If we allow the pole of each composition plane, IB-1, IB-2 and IB-3 be IB(1), IB(2) and IB(3), the azimuthal angle, one of the two remaining DOFs, can then be determined from the SEM image shown in Fig. 1(*a*), namely 3° for IB-2 and 27° for IB-3 clockwise from *N* as shown in Fig. 3. Note that the pIB(1), pIB(2) and pIB(3) denote respectively the projected poles of IB(1), IB(2) and IB(3) on the polished sample surface.

It follows that the non-basal portions of the IB can be characterized completely once the last remaining DOF, *i.e.* the polar angle, is specified. However, it is unfortunate that no reliable macroscopic technique for the purpose has been developed yet. It is mainly because the determination of the polar angle can only be possible when the three-dimensional information on the specimen is available. Although the required information may be collected through a systematic serial sectioning procedure from the theoretical point of view (Saylor *et al.*, 2003), this technique is subject to a large range of errors from the practical point of view. For special solid/solid interfaces which are expected to assume a low Miller index, however, a precise characterization is possible by applying the classical crystallographic technique as will be demonstrated below.

Fig. 4(*a*) shows a part image of Fig. 2(*b*) containing IB-2. As is indicated in this figure, the normal direction of the projection plane is $(2\bar{1}\bar{1}2)$ from the EBSD analysis, and that of the IB-2 is IB(2) following the previous notation. The details of

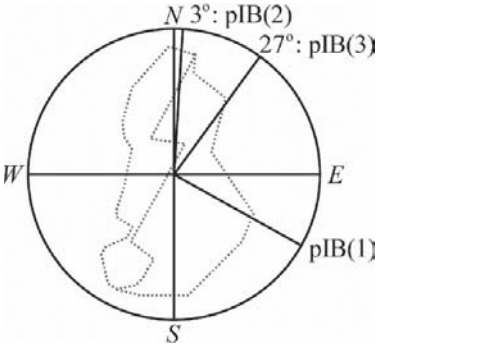

Figure 3
A schematic illustration showing the azimuthal angles measured from the SEM image in Fig. 1(*a*). Angles were measured from a reference point denoted by *N* to each pole of IB clockwise.

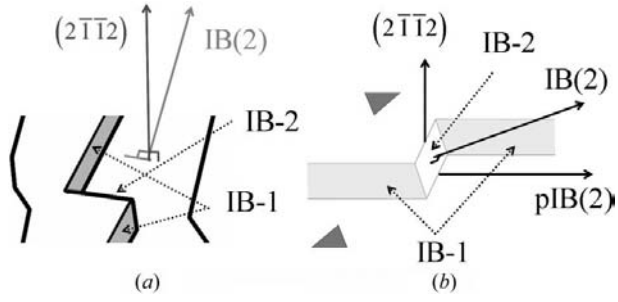

Figure 4
(*a*) A part image near IB(2) from Fig. 2(*b*) illustrating the meaning of pIB(2). (*b*) A schematic clinographic view of (*a*) showing all the related poles for the complete analysis on IB(2).

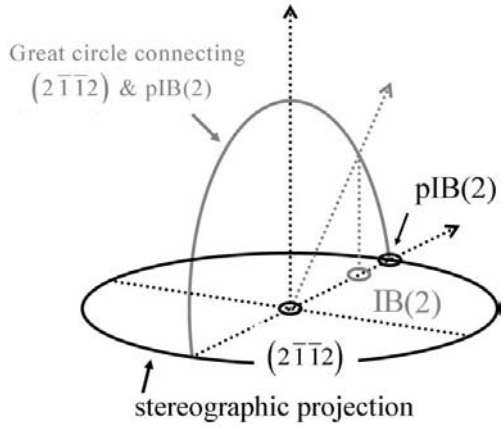

Figure 5
A schematic illustration demonstrating basic procedure employed in the current analysis. Note that the crystallographic identification of IB(2) is tractable once the great circle connecting the pole of $(2\bar{1}\bar{1}2)$ and pIB(2) poles is determined.

the notation can be referred to a clinographic image of Fig. 4(*a*) (see Fig. 4*b*). Then, it is quite evident that all three poles, $(2\bar{1}\bar{1}2)$, IB(2) and pIB(2), should lie in a common plane. In other words, IB(2) should be on the trace of a great circle passing through the two poles of $(2\bar{1}\bar{1}2)$ and pIB(2). Therefore, the location of IB(2) on the stereographic projection will be somewhere between the origin and pIB(2) on the line passing through the origin on the stereographic projection as is shown in Fig. 5, since the great circles are always represented by a line segment passing through the origin on the standard stereographic projection.

In addition, the position of IB(2) can be further specified to be very near to pIB(2) on the stereographic projection. Notice that IB-2 and IB-3 are almost perpendicular to the projection plane (see Fig. 2*b*). In the mean time, if one recalls that the inversion boundary is a special twin plane and should satisfy the inversion symmetry constraint, it should be one of the low-index planes near the edge of the projection plane.

Since the standard $(2\bar{1}\bar{1}2)$ projection of ZnO is not available from the literature, it was constructed by an appropriate modification on the standard (0001) projection as follows. The standard (0001) projection of ZnO crystal system whose $c/a = 1.60$ was first constructed by calculating the interplanar angles between major poles of the hexagonal system, and was rotated about the $(0\bar{1}10)$ axis to locate the pole of $(2\bar{1}\bar{1}2)$ at the origin.

In the mean time, the pole figure in Fig. 2(*a*) was superimposed by the standard Wulff net with 1° interval as is presented in Fig. 6(*a*). To locate a reference pole *N* on the standard $(2\bar{1}\bar{1}2)$ projection, the angular distance of 112° was measured from the great circle passing *N* and (0001) using the Wulff net. Then, *N* was marked on the constructed standard $(2\bar{1}\bar{1}2)$ projection, which was superimposed by the standard Wulff net rotated to satisfy the interplanar angle between (0001) and *N* to be 112° as shown in Fig. 6(*b*). The pIB(2), which is 3° away from *N*, and the pIB(3), which is 27° away from *N*, are also marked on it.

As was discussed in Fig. 5, the determination of the last remaining DOF, the polar angle, for IB-2 and IB-3 simply requires finding the proper great circle passing through $(2\bar{1}\bar{1}2)$ pole and pIB(2) (Fig. 6*a*) and the great circle passing through $(2\bar{1}\bar{1}2)$ and pIB(3) (Fig. 6*b*) by rotating the Wulff net in an appropriate manner.

In the case of IB(2), there exist two possible choices, $\{2\bar{2}01\}$ and $\{01\bar{1}1\}$,[1] as shown in Fig. 7(*a*). Besides, the polar angles between pIB(2) and the nearest poles, $\{01\bar{1}1\}$ and $\{2\bar{2}01\}$, are about 14 and 58°, respectively. From the SEM image shown in Fig. 1(*a*), the IB(2) can be determined to be $\{01\bar{1}1\}$. The relevance of the choice of the $\{01\bar{1}1\}$ plane as a composition plane of IB is supported by the observation of the $\{01\bar{1}1\}$ plane at the irregular inversion boundary of Ti-doped ZnO (Makovec & Trontelj, 1994).

[1] Although the correct choice of the pole IB(2) should be $(01\bar{1}1)$ in the projection, a safe way to describe the correct pole may be referred to the corresponding planes of a form, since the initial choice of $(2\bar{1}\bar{1}2)$ was an arbitrary choice from the planes of a form.

In the same way, IB(3) can be determined among the two possible choices, *i.e.* $\{0\bar{1}10\}$ and $\{1\bar{2}11\}$. Details of the procedure are illustrated in Fig. 7(*b*). It is evident that IB(3) is $\{0\bar{1}10\}$, since the polar angle between pIB(3) and $\{0\bar{1}10\}$ and $\{1\bar{2}11\}$ are about 0 and 34°, respectively. It is interesting to note that the $\{0\bar{1}10\}$ composition plane is a part of IB, although it is crystallographically non-polar. In the case of GaN grown on sapphire, this type of composition plane in IB has been observed and confirmed to have an inversion symmetry (Rouviére *et al.*, 1995; Potin *et al.*, 1997). One thing to be noted is that the extent of the $\{0\bar{1}10\}$ composition plane found in GaN is at most 40 nm, which is too small to be observed macroscopically. This limited size was attributed to a relatively high energy of the boundary due to a different bonding strength between Ga—Ga and N—N wrong bonds at the boundary (Potin *et al.*, 1997).

However, the extent of the $\{0\bar{1}10\}$ composition plane found in the current analysis is substantial enough to be observed

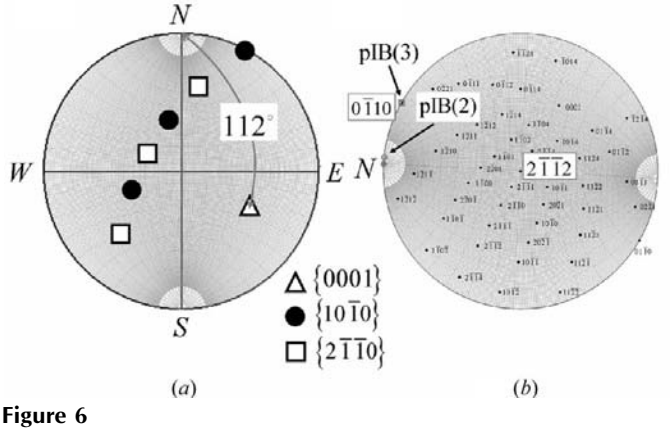

Figure 6
(*a*) The stereographic projection from Fig. 2(*a*), superimposed by the standard Wulff net. (*b*) The standard $(2\bar{1}\bar{1}2)$ projection with the concerning poles. (For simplicity, the parentheses for the pole notation on the standard projection are omitted.)

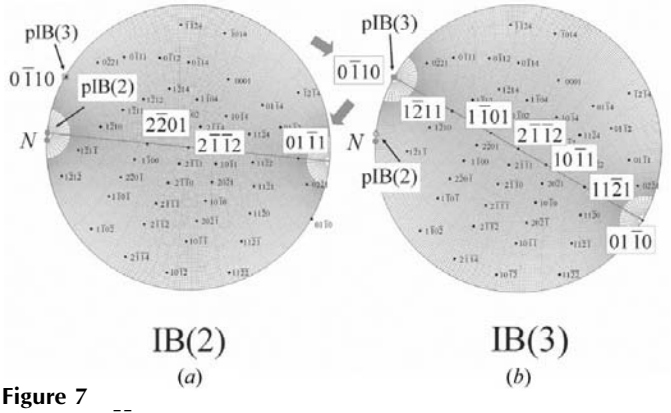

Figure 7
Standard $(2\bar{1}\bar{1}2)$ projection, which shows the great circle of connecting $(2\bar{1}\bar{1}2)$ pole with (*a*) pIB(2) and (*b*) pIB(3), based on the measured azimuthal angle. The poles of interest, IB(2) and IB(3), should be respectively near pIB(2) and pIB(3) on the line. (For simplicity, the parentheses for the pole notation on the standard projection are omitted.)

even with an optical microscope. This implies that the energy of the $\{0\bar{1}10\}$ composition plane in ZnO should be comparable with that of the other two composition planes. As the bond strength between Zn—Zn and O—O wrong bonds in ZnO should also be different, the boundary structure of the $\{0\bar{1}10\}$ composition plane in ZnO at an atomistic level should be significantly different from that in GaN. In addition, the physicochemical properties of $\{10\bar{1}0\}$ could be significantly different from the other two composition planes, (0001) and $\{01\bar{1}1\}$. It follows that a detailed analysis on the atomic structure of the $\{10\bar{1}0\}$ composition plane through TEM is needed to obtain a better understanding of IB in ZnO.

4. Conclusions

Crystallographic analysis on the composition planes in the Sb-induced inversion boundaries of ZnO was performed. Statistical observation on the microstructure revealed that there exist three different types of composition planes in the inversion boundary including the basal one. All five macroscopic DOFs for describing general grain boundaries crystallographically were determined by the application of EBSD and the stereographic projection technique. The results revealed that the composition planes of IB are (0001), $\{10\bar{1}0\}$ and $\{10\bar{1}1\}$. The currently developed simple and intuitive method is expected to be applied to analyze the inversion boundaries in other polar crystals.

This work was supported by the Ministry of Education & Human Resources Development of the Korean Government through the Brain Korea 21 Project.

References

Austerman, S. B. (1962). *Bull. Am. Phys. Soc. Ser. II*, **7**, 607.
Chung, U.-J., Jo, W., Lee, J.-H., Hwang, N.-M. & Kim, D.-Y. (2004). *J. Am. Ceram. Soc.* **87**, 125–128.
Chung, U.-J., Park, J.-K., Hwang, N.-M., Lee, H.-Y. & Kim, D.-Y. (2002*a*). *J. Am. Ceram. Soc.* **85**, 965–968.
Chung, U.-J., Park, J.-K., Hwang, N.-M., Lee, H.-Y. & Kim, D.-Y. (2002*b*). *J. Am. Ceram. Soc.* **85**, 3076–3080.
Daneu, N. & Bernik, S. (2001). *J. Eur. Ceram. Soc.* **21**, 1879–1882.
Daneu, N., Rečnik, A. & Bernik, S. (2003). *J. Am. Ceram. Soc.* **86**, 1379–1384.
Daneu, N., Rečnik, A., Bernik, S. & Kolar, D. (2000). *J. Am. Ceram. Soc.* **83**, 3165–3171.
Holt, D. B. (1969). *J. Phys. Chem. Solids*, **30**, 1297–1308.
Jo, W., Kim, S.-J. & Kim, D.-Y. (2005). *Acta Mater.* **53**, 4185–4188.
Kang, M.-G. & Kim, D.-Y. (2000). *J. Am. Ceram. Soc.* **83**, 3202–3204.
Kang, M.-K., Yoo, Y.-S., Kim, D.-Y. & Hwang, N.-M. (2000). *J. Am. Ceram. Soc.* **83**, 385–390.
Kim, J. C. & Goo, E. (1990). *J. Am. Ceram. Soc.* **73**, 877–884.
Makovec, D. & Trontelj, M. (1994). *J. Am. Ceram. Soc.* **77**, 1202–1208.
Morizane, K. (1977). *J. Cryst. Growth*, **38**, 249–254.
Petroff, P. M. (1986). *J. Vac. Sci. Technol. B*, **4**, 874–877.
Pirouz, P. & Powell, J. A. (1987). *Appl. Phys. Lett.* **50**, 221–223.
Potin, V., Ruterana, P. & Nouet, G. (1997). *J. Appl. Phys.* **82**, 2176–2183.
Rečnik, A., Daneu, N., Walther, T. & Mader, W. (2001). *J. Am. Ceram. Soc.* **84**, 2657–2668.
Romano, L. T., Robertson, I. M., Greene, J. E. & Sundgren, J. E. (1987). *Phys. Rev. B*, **36**, 7523–7528.
Rouviére, J. L., Arlery, M., Bourret, A., Niebuhr, R. & Bachem, K. M. (1995). *Inst. Phys. Conf. Ser.* **146**, 285–288.
Saylor, D. M., Morawiec, A. & Rohrer, G. S. (2003). *Acta Mater.* **51**, 3675–3686.
Senda, T. & Bradt, R. C. (1991). *J. Am. Ceram. Soc.* **74**, 1296–1302.
Snykers, M., Delavignette, P. & Amelinckx, S. (1971). *Mater. Res. Bull.* **7**, 831–839.
Yoo, Y.-S., Kim, H. & Kim, D.-Y. (1997). *J. Eur. Ceram. Soc.* **21**, 805–811.